SURFACE DEFORMATION EFFECTS ON THE FREE-SURFACE TURBULENCE STRUCTURE IN HIGH-Fr OPEN-CHANNEL FLOW

Yoshinobu Yamamoto
Dept, Energy eng. and sci., Nagoya University
Chikusa Furo Nagoya, 464−8603, Japan
y-yamamoto@nucl.nagoya-u.ac.jp

Tomoaki Kunugi
Dept. Nuclear eng.,Kyoto University
Yoshida Sakyo Kyoto, 606-8501, Japan
kunugi@nucleng.kyoto-u.ac.jp

Shin-ichi Satake
Dept. Applied Electronics, Tokyo University of Science
Yamasaki Noda Chiba, 278−8510, Japan
satake@te.noda.tus.ac.jp

ABSTRACT

In this study, we succeed in a direct numerical simulation (DNS) of a high-Fr turbulent open-channel flow at a Froude number of 1.8 and a Reynolds number of 2325 based on a bulk velocity, the gravity acceleration, a water depth and the kinetic viscosity, by means of the multi-interfaces advection and reconstruction solver (MARS) method, and the DNS database such as the mean velocity, turbulent statistics and surface fluctuations were obtained. At the free-surface, surface waves are constructed of large-scale gently bumped waves with the maximum wave-height approximately corresponding to 4% of the water depth and the small scale isotropic waves caused by surface fluctuations. Wall-normal turbulent intensity and energy-dissipation rate were increased toward the free-surface. These tendencies of turbulent statistic quntities near the free-surface were in good agreement with experimental measurement results by using a laser doppler anemometer (LDA) (Nakayama and Nezu, 1999). Although increase of vertical turbulent intensity, the redistribution of turbulent intensity from vertical component to streamwise one is predominant near free-surface in high-Fr flow. It is similar to a low-Fr flow.

INTRODUCTION

Free-surface turbulence has been investigated extensively both experimentally and numerically (Komori et.al., 1982, Lam and Banerjee, 1992, Nezu and Nakagawa, 1993, Handler et. al., 1993, Nagaosa, 1999). In open-channel turbulent flows, which might be imaged as river flows or liquid-film flows, the Froude number [$\mathrm{Fr}=U/(gh)^{1/2}$, where U is bulk mean velocity, g is gravity acceleration and h is flow depth, respectively] is an important factor for free-surface deformation effects on turbulence structures. In low-Fr range ($\mathrm{Fr}<0.5$), the surface deformation is small. Rigid-lid free-surface acts like a wall and restrains on surface-normal velocity component. On the other hand, in high-Fr range ($Fr>1.0$), the tendency of surface-normal turbulent intensity increase was measured by using a LDA(Nezu and Nakagawa, 1993, Nakayama and Nezu, 1999). It showed that surface deformation effects could be neglected no longer and free-surface turbulence structures being different from a low-Fr flow would be expected in high-Fr flow. In the view points of understanding coherent structures and high-ordered turbulent statistics behavior (e.g., vortex, energy-dissipation rate and pressure-strain term), the DNS is expected to have advantages of the experimental approaches. But, most of DNS in turbulent open-channel flows have been carried out under zero or low-Fr flow condition(Lam and Banerjee, 1992, Handler et. al., 1993, Komori et. al., 1993, Nagaosa, 1999, Borue et. al., 1995, Thomas and Williams, 1995, Yokojima, 2002).

NUMERICAL PROCEDURE AND NUMERICAL CONDITIONS

Numerical procedure was based on the MARS method (Kunugi, 1997, Kunugi, 2001); the governing equations are consisted of Navier-Stokes equations with the CSF (Continuum Surface Force) model (Brackbill, 1992) , continuity equation and transport equations of a volume fraction function (VOF) F. As for the discretization of the governing equations on the Cartesian coordinate system, the second-order scheme for the spatial differencing terms is used on the staggered grid system and the Euler implicit scheme is used for the first stage of projection method to solve the momentum equation. The physical problem treated here is the motion of two Newtonian incompressible fluids allowed the interface deformation between them.

The schematic view of a high-Fr open-channel flow at Fr=1.8, is shown in Fig.1-1 and the numerical conditions are tabled in Table 1. Compared with the high-Fr case, DNS of a Zero-Fr (e.g., rigid-lid) open-channel flow shown in Fig.1-2 and a parallel channel flow in Fig.1-3 were carried out. As the bounday conditions, periodic boundary conditions in the spanwise (x) and streamwise (z) directions are imposed, the no-slip condition is applied to upper gas boundary and lower water boundary, respectively. As the initial conditions, the water surface was flat, the velocity field for water layer was used in the rigid-lid case data and the gas layer velocity set zero, respectively. Constant streamwise mass flux

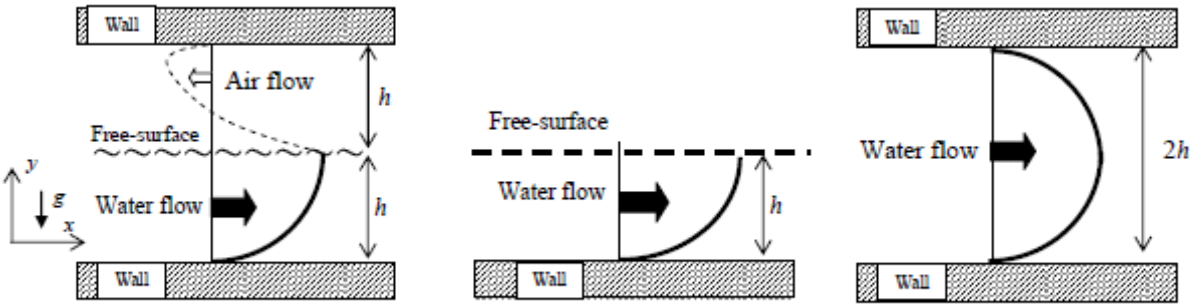

Fig.1-1 High-Fr open-channel flow Fig.1-2 Rigid-lid open-channel flow Fig.1-3 Paralle channel flow

Fig.1 Schematic view of the present flow fields

Table 1 Numerical condition

	Re_τ	Fr	ρ_w/ρ_g	Domain $L_x \times L_y \times L_z$	Grid number $N_x \times N_y \times N_z$	Resolution $\Delta x^+, \Delta y^+, \Delta z^+$	T_0^+	T_m^+
CASE1	150	1.8	842.1	$12.8h \times 2h \times 6.4h$	384×214×192	5.0, 0.26-2.0, 5.0	610	630
CASE2	150	0	-	$12.8h \times h \times 6.4h$	384×107×192	5.0, 0.26-2.0, 5.0	-	800
CASE3	150	-	-	$12.8h \times 2h \times 6.4h$	384×182×192	5.0, 0.26-2.0, 5.0	-	800

CASE1 (Super-critical open-channel flow): $Re_\tau = u_\tau h/\nu_w$: Turbulent Reynolds number, u_τ: Friction velocity at bottom wall, h: water depth(=Gas layer height), ν_w: Kinetic viscosity of water, $Fr = U_m h/\nu_w$: Froude number, U_m: Bulk mean velocity in water side, ρ_w : liquid density, ρ_g : Air density, L_x, L_y, L_z: Computational domain, N_x, N_y, N_z: Grid number, $\Delta x^+, \Delta y^+, \Delta z^+$: Grid resolution for stream (x)-, vertical (y)-, and span (z)- wise directions, respectively. Super-script + denotes the nondimensional quantities normalized by friction velocity and kinetic viscosity used Reynolds number definition. T_0^+: Time integration length from initial condition to fully-developed status, T_1^+: Time integration length after fully-developed status.CASE2 and 3 (Rigid-rid open-channel flow and Parallel channel flow): $Re_\tau = u_\tau h/\nu_w$: Turbulent Reynolds number, u_τ: Friction velocity at the wall, h or $2h$: water depth.

condition was imposed for each of water- and gas-phase to keep the initial momentum flux difference between gas- and water-phases. Consequently, the bulk Reynolds number in water phase was 2325 in high-Fr case.

RESULTS AND DISSCUSSION

Figures 2-1 and 2 show the R.M.S. of VOF function F and Fig. 3 shows the instantaneous water-surface profile in high-Fr open-channel flow. Profiles of R.M.S. of F depict almost symmetrical and maximum wave-height, which was resolved on 20 grids in y-direction, is approximately corresponding to the 4% of the water depth. Gently bumped large-scale waves and high-frequency fluctuations on them are observed in Fig. 3.

Figures 4 and 5 show the mean velocity and the turblent intensity profiles in high-Fr and low-Fr cases, respectively. These data were averaged at the height from bottom wall: air-phase does not distinguished from water-phase. In the high-Fr case, air- and water-side flows into countercurrent direction each other except for near free-surface of air-side flow as shown in Fig.4-1. Mean velocity profile of the air-side flow shows a parabolic shape. This means that the air-side flow is not turbulent flow but laminar flow. Turbulent intensity profiles shown in Fig.5-1 have the peaks at the free-surface caused from surface deformation effects. In low-Fr case, as pointed out in previous works (Komori et.al., 1982, Lam and Banerjee, 1992, Nezu and Nakagawa, 1993, Handler et. al., 1993, Nagaosa, 1999), wall-normal turbulent intensity was suppresed by the presence of the rigid-lid free-surface.

Instantaneous streamwise-velocity conters in CASE1 (high-Fr case) were shown in Figs.6-1 (side view) and -2 (end view), respectively. In the water side, the typical turbulent shear flow was formed. On the other hand, the velocity range in the air side were constant compared with the wataer side. These indicate that the air-liquid interface interaction were inactive and the present flow field in CASE1 was considerd just “open-channel flow“.

Figures 7-1,-2 and -3 show the streamwise turbulent velocity distributions in the case of high-Fr condition near the bottom wall (y^+=14.5), near the free-surface (y^+=138.5) and at the free-surface (y^+=149.7), respectively. Near the bottom wall, typical wall turbulent structures organaized by the high- and low-speed streks were observed, and the most of turbulence were produced in this region as well as the low-Fr open-channel flow. There were no gas-phase area on the velocity distributions near the free-surface as shown in Fig.7-2. Some low-velocity area were observed. This might be related to the surface renewal vortices (Komori et.al., 1982, Lam and Banerjee, 1992, Nezu and Nakagawa, 1993, Handler et. al., 1993, Nagaosa, 1999). At the free-surface as shown in Fig.7-3, both gas and water phases existed and the low speed areas painted with black were coresponding to the gas-phase areas. High-frequency fluctuations are observed in the high-speed areas painted white. Large high-frequency fluctuations areas on warer-surface profile can be seen.

Figures 8-1, -2 and -3 show the energy spectrum profiles of turbulent velocity componets in high-Fr case, near the bottom wall (Fig.8-1) and near the free-surface

(Figs. 8-1 and 2), respectively. Near the bottom wall, the surface deformation effect on them cannot be observed, but near the free-surface it was apperaed clearly in the high-wave region.

Figure 9 shows the near free-surface mean velocity profiles distinguished air-phase from water-phase. Mean velocity profile in the water-phase is almost constant and the air-phase profile has the velocity gradient like a boundary layer profile. This means that momentum transfer from water-phase to air-phase might be active, but the momentum transfer from air-phase to water-phase might be inactive.

Figure 10 shows the water-phase turbulent intensity profiles in all cases. In high-Fr case, near the free-surface (y^+>140) vertical turbulent intensity begins to increase up to the free-surface and the vertical confinement effect(Komori et. al., 1982, Lam and Banerjee, 1992, Nezu and Nakagawa, 1993, Handler et. al., 1993, Nagaosa, 1999) might be no longer present. This indicates that the near free-surface turbulence is caused from free-surface instabilities. On the other hand, the streamwise and spanwise turbulent intensities are decreased compared with low-Fr case. Turbulent intensities scale in high-Fr case is closed to the parallel channel center values. The tendency of vertical turbulent intensity increase near the free-surface were similar to the experimental measurement results with a LDA by Nakayama and Nezu, 1999.

Figure 11 show the water-phase tubulent kinetic energy. In high-Fr case compared with low-Fr one, turbulent kinetic energy were decresed. This migh be caused from the energy transfer from the water-phase to the gas-phase.

Figure 12 show the water-phase energy-dissipation rate profile. Energy dissipation rate near the free-surface is increased in high-Fr case. On the other hand, the energy dissipation rate in low-Fr case is slightly decreased. Tendency of energy-dissipation rate incrfease near the free-surface were also reported by Nakayama and Nezu, 1999. Although the energy disspation rate was not mesured directly, they estimated it from the spectrum profile gradient on the experimental measurements.

Figure 13 shows the pressure-strain term distribution in all cases, where φ_{11}, φ_{22}, φ_{33} denotes stremwise, vertical and spanwise pressure-strain term, respectively. Near the free-surface in high-Fr case, the redistribution from vertical component to streamwise one, as for low-Fr case, from vertical one to others, and in paralle channel flow case, from streamwise to others are dominant, respectively. In low-Fr case, the redistribution of vertical componet to others is depended on the decrese of vertical intensity. On the other hand, in high-Fr case, even though increase of vertical intensity, the redistribution from vertical component to streamwise one is also dominant. It might indicate that the surface deformation is related to the largest turbulent componet i.e. streamwise one and vertical component are supplied only from the free-surface. Consequently the redistoribution from veartical componet to streamwise one is dominat under the free-surface.

SUMMARY

In this study, the direct numerical simulation of a high-Fr turbulent open-channel flow at a Froude number of 1.8, were conducted by means of the MARS method. DNS database such as the mean velocity, turbulent statistics and surface fluctuations were obtained and near free-surface turbulent structures at high-Fr flow was investigated compared with low-Fr flow. The follwing results are obtained;

1) At the free-surface, surface waves are constructed of large-scale gently bumped waves with the maximum wave-height approximately corresponding to 4% of the water depth and the small scale isotropic waves caused by surface fluctuations.
2) Near the free-surface, wall-normal turbulent intensity and energy-dissipation rate were increased.
3) On the ohter hand, near free-surface turbulent kinetic energy in high-Fr flow compared with a low-Fr flow were decresed.
4) Turbulent statistic tendencies near the free-surface were in good agreement with the experimental measurement results by using a Laser Doppler Anemometer (Nakayama and Nezu, 1999).
5) Near the free-surface in high-Fr flow, turbulent redistribution from vertical component to streamwise one is dominant. Although the increase of vertical intensity, it is similar to a low-Fr flow. This might be the reason why the surface deformation is related to the streamwise turbulent component and the vertical component is supplied only from the surface deformation. Consequently, the redistoribution from veartical componet to streamwise one is dominat under the free-surface.

ACKNOWLEDGEMENT

A part of the present study is the result of "Development of a high-precision numerical simulator based on the computer science approach for the evaluation of gas inclusion in FBR" entrusted to Nagoya Univ. by the Ministry of Education, Culture, Sports, Science and Technology of Japan (MEXT). Prsent numerical calculations were conducted by using the Earth Simulator at JAMSTEC and HPC2500 at Information Technology Center, Nagoya Univ.

REFERENCES

Borue. V, et al. J. Fluid Mech., 286(1995), pp.1-23.

Brackbill, J.U. et al, J. Comput. Phys., 100(1992), pp.335-354.

Komori, S. et al., Int. J. Heat Mass Transfer, 25-4(1982), pp.513-521.

Komori , S, et al., Phys. Fluids, A5(1993), pp.115-125.

Komori, S. et al., Int. J. Heat Mass Transfer, 25-4(1982), pp.513-521.

Kunugi, T., Trans. JSME Ser. B, vol.63, no. 609(1997), pp.1576-1584.[in Japanese].

Kunugi, T., Comput. Fluid Dynamics J., vol.9, no.1 (2001), pp. 563-571.

Handler, R.A. et al., AIAA J, 31-11(1993), pp.1998-2007.

Lam, K. and Banerjee, S., Phys. Fluids, A4(1992), pp.306-320.

Nagaosa, R., Phy. Fluids, 11-6(1999), pp.1581-1595.

Nakayama, T and Nezu, I , J. Hydraulic, Costal and Environmental Eng. JSCE, 635/ Ⅱ -49(1999) , pp.31-40.[in Japanes].

Nezu, I. and Nakagawa. H., Turbulence in Open-Channel Flows, A.A. Balkema, Rotterdam(1993).

Thomas, T.G. and Williams, J.R., Int. J. Heat Mass Transfer, 38-2.(1995), pp.259-266.

Yokojima, S. PhD thesis, Kobe Univ. (2002).

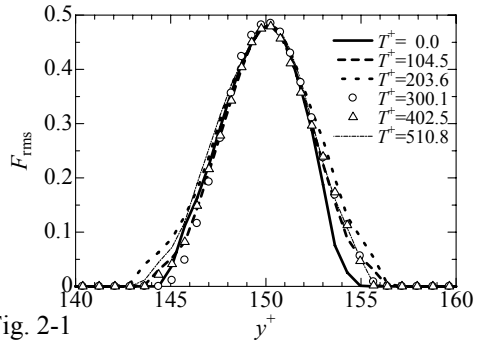

Fig. 2-1

R.M.S. of VOF function profiles' time history, near the free-surface (Fr=1.8)

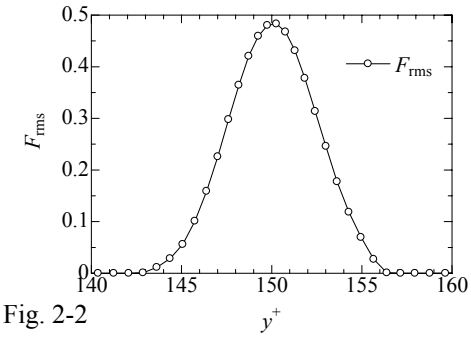

Fig. 2-2

R.M.S. of VOF function profile, near the free-surface (Fr=1.8)

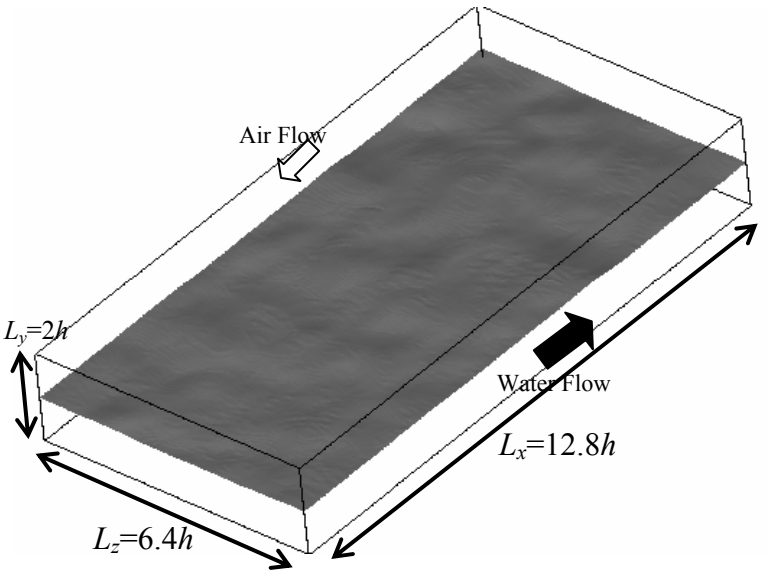

Fig. 3 Instantaneous free-surface, bird view (Fr=1.8)

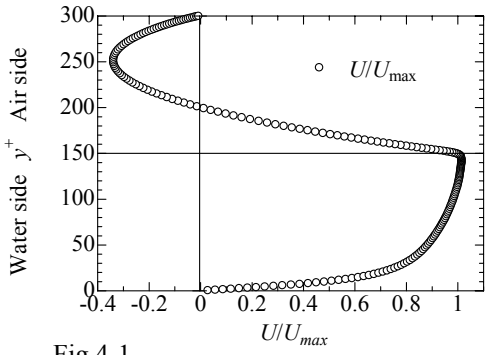

Fig.4-1

Mean velocity distribution, (Fr=1.8)

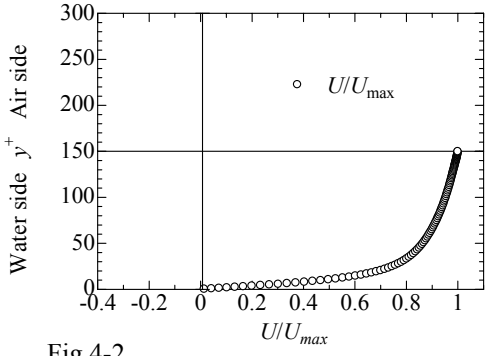

Fig.4-2

Mean velocity distribution (Fr=0.0)

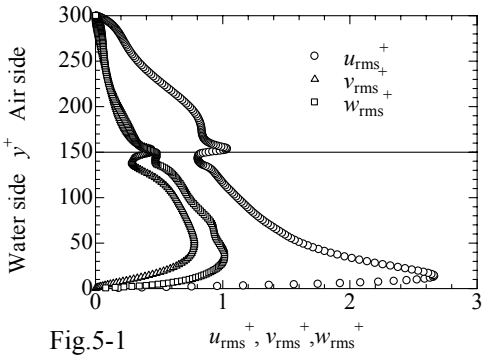

Fig.5-1

Turbulent intensity profiles, Fr=1.8

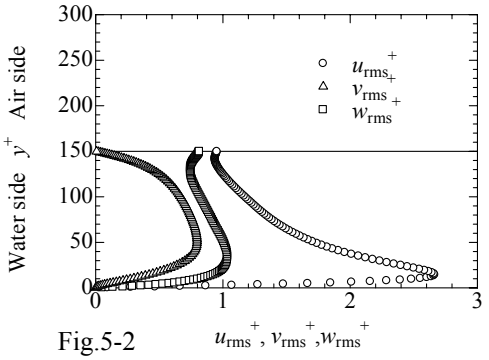

Fig.5-2

Turbulent intensity profiles, Fr=0.0

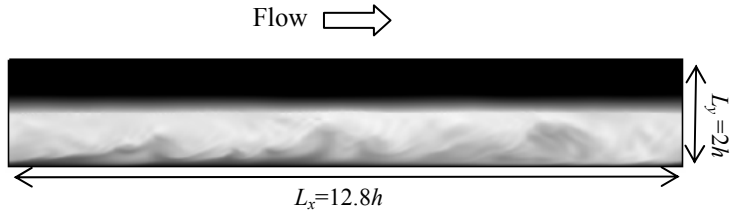

Fig.6-1 Streamwise velocity distribution, side view
0.0(Black)<U^++u^+<20.1(White)

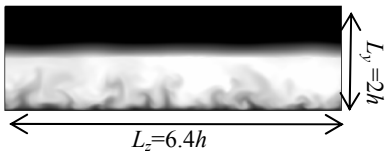

Fig.6-2 Streamwise velocity distribution,
end view,0.0(Black)<U^++u^+<18.7(White)

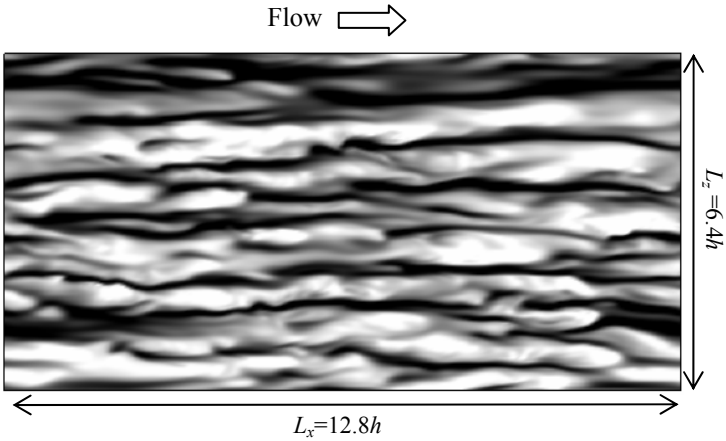

Fig.7-1 Streamwise turbulent velocity distribution, top view,
near wall, -3.7(Black)< u^+<3.7(White), y^+=14.5

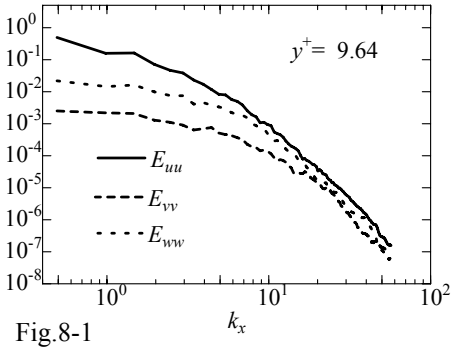

Fig.8-1
Streamwise-energy spectra, near wall
(Fr=1.8)

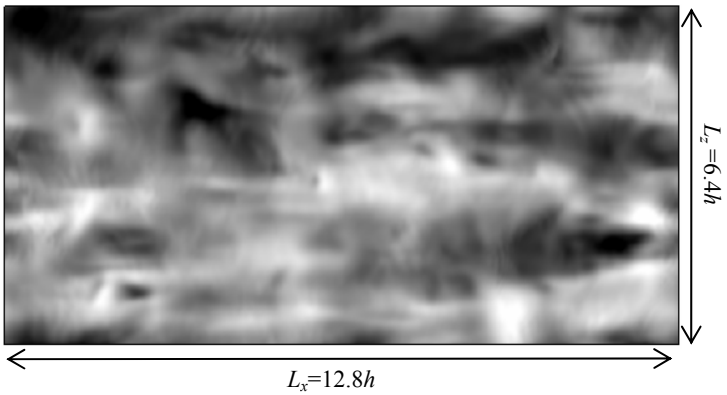

Fig.7-2 Streamwise turbulent velocity distribution, top, view
, near the free-surface, -1.9(Black)< u^+< 1.9(White), y^+=138.5

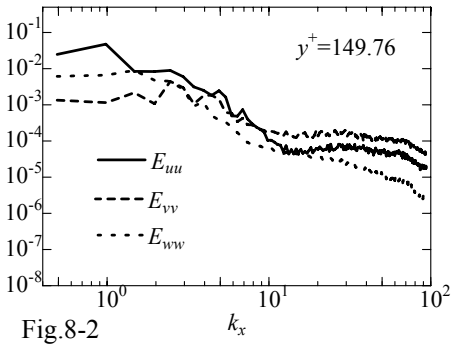

Fig.8-2
Streamwise-energy spectra at the free-surface
(Fr=1.8)

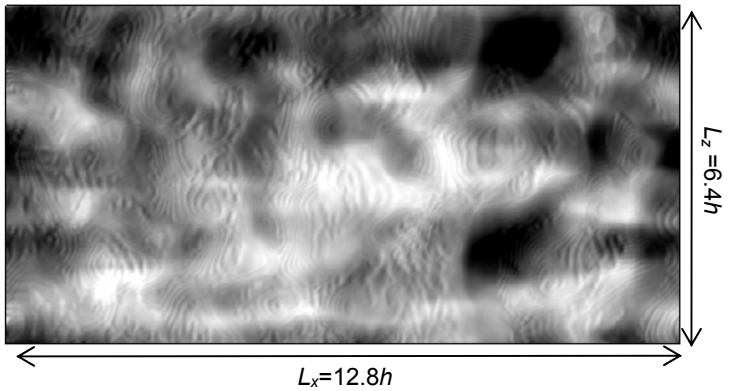

Fig.7-3 Streamwise turbulent velocity distribution, top, view,
at the free-surface, -1.9(Black)< u^+< 1.9(White), y^+=149.7

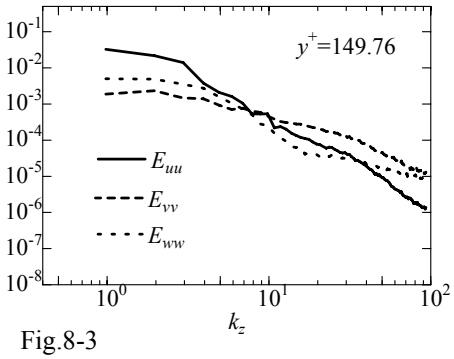

Fig.8-3
Spanwise-energy spectra at the free-surface
(Fr=1.8)

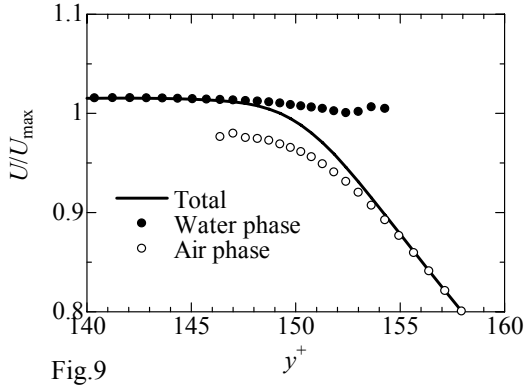

Fig.9
Mean velocity distributions, near the free-surface
(Fr=1.8)

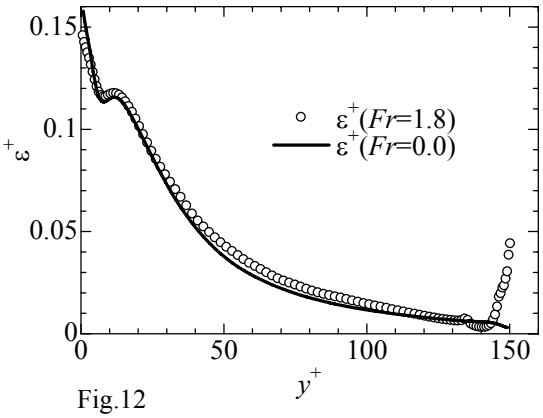

Fig.12
Turbulent energy dissipation distributions
(Water phase)

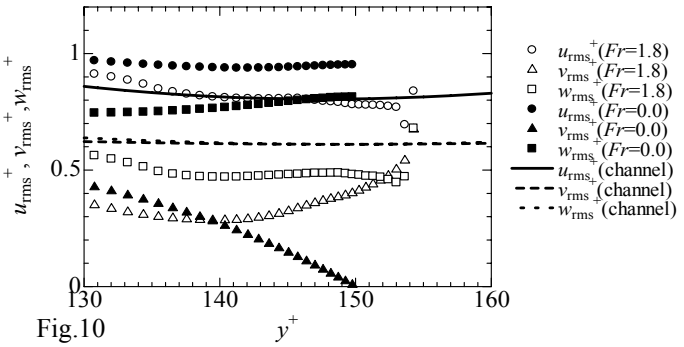

Fig.10
Turbulent intensity profiles, near the free-surface

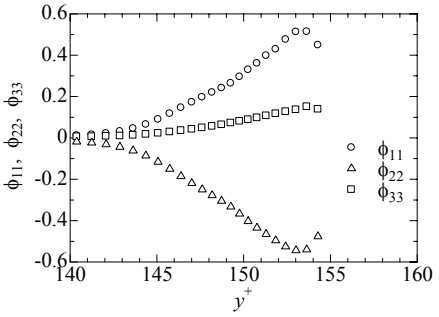

Pressure-strain term distributions, near the free-surface
(Fr=1.8, Water-phase)

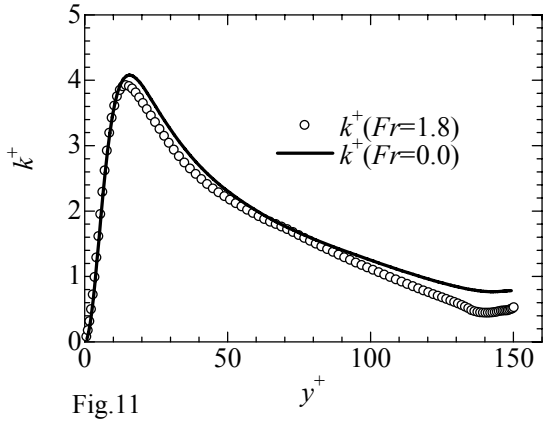

Fig.11
Turbulent kinetic energy distributions
(Water phase)

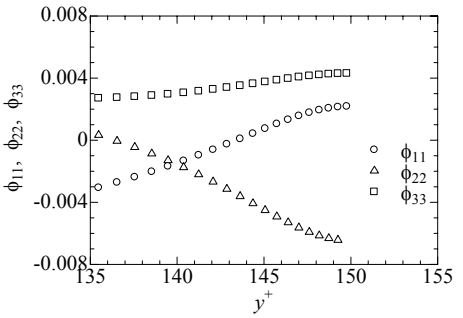

Pressure-strain term distributions, near the free-surface
(Fr=0.0)

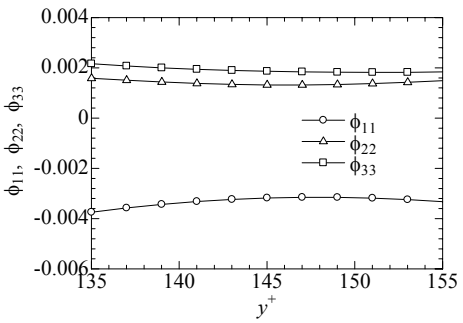

Pressure-strain term distributions,
near the channel center

Fig.13 Pressure-strain term distribution